JOURNAL OF GEOPHYSICAL RESEARCH, VOL. 115, A00G01, doi:10.1029/2009JA015188, 2010

Ionospheric variability due to planetary waves and tides for solar minimum conditions

H.-L. Liu,[1] W. Wang,[1] A. D. Richmond,[1] and R. G. Roble[1]

Received 13 December 2009; revised 10 February 2010; accepted 18 February 2010; published 29 June 2010.

[1] Large ionospheric variability is found at low to middle latitudes when a quasi-stationary planetary wave is specified in the winter stratosphere in the National Center for Atmospheric Research thermosphere-ionosphere-mesosphere electrodynamics general circulation model for solar minimum conditions. The variability includes change of electric field/ion drift, F2 peak density and height, and the total electron content. The electric field/ion drift change is the largest near dawn in the numerical experiments. Analysis of model results suggests that, although the quasi-stationary planetary wave does not propagate deep into the ionosphere or to low latitudes due to the presence of critical layers and strong molecular dissipation, the planetary wave and tidal interaction leads to large changes in tides, which can strongly impact the ionosphere at low and middle latitudes through the E region wind dynamo. Large zonal gradients of zonal and meridional winds from the tidal components and the zonal gradient of electric conductivities at dawn can produce large convergence/divergence of Hall and Pedersen currents, which in turn produces a polarization electric field. The ionospheric changes are dependent on both the longitude and local time, and are determined by the amplitudes and phases of the superposing wave components. The model results are consistent with observed ionospheric changes at low and middle latitudes during stratospheric sudden warming events, when quasi-stationary planetary waves become large.

Citation: Liu, H.-L., W. Wang, A. D. Richmond, and R. G. Roble (2010), Ionospheric variability due to planetary waves and tides for solar minimum conditions, *J. Geophys. Res.*, *115*, A00G01, doi:10.1029/2009JA015188.

1. Introduction

[2] The Earth's ionosphere has significant day-to-day variability and displays oscillations over a wide range of timescales. The regular daily, 27 day (solar rotation period), and seasonal variations are caused by the change of photoionization associated with changes of solar radiation and solar zenith angle. Profound ionospheric changes also result from geomagnetic storms and substorms, which can last for hours and it can take days for the ionosphere to recover. Even during nonstorm period, geomagnetic perturbations associated with solar coronal holes and high-speed solar wind streams can cause periodic ionosphere and thermosphere oscillations with the solar rotation period and subharmonics of this period [*Lei et al.*, 2008]. Statistical studies also establish correlation between ionospheric variability and the Kp or Ap index [*Rishbeth and Mendillo*, 2001; *Pancheva et al.*, 2002; *Altadill and Apostolov*, 2003; *Xiong et al.*, 2006].

[3] Ionospheric day-to-day variability is also observed under geomagnetically undisturbed conditions. For instance, *Rishbeth and Mendillo* [2001] found that, for medium solar activity, the daily fluctuations of the ionospheric peak electron density (NmF2) have a standard deviation of 20% in the daytime and 33% in the nighttime. Using data from over 100 ionosonde stations, *Forbes et al.* [2000] showed that under very quiet conditions (Kp < 1), the standard deviation or $1-\sigma$ variability of NmF2 about the mean was about 25–35% at high frequencies (periods of a few hours to 1–2 days) and about 15–20% at low frequencies (periods of 2–30 days) at all latitudes. *Mikhailov et al.* [2004, 2007] also showed that there exist synchronous quiet day electron density variations in both the E and F regions. The variations of NmF2 can be more than 40% from its mean values. Recent observations by C/NOFS have revealed very large equatorial ionospheric depletion near dawn under geomagnetically quiet conditions [*de La Beaujardière et al.*, 2009]. The ionospheric daily variability during these geomagnetically quiet periods has been suggested to be caused by perturbations originating from the lower atmosphere [*Chen*, 1992; *Rishbeth and Mendillo*, 2001]. These perturbations are most likely tied to atmospheric waves, including atmospheric tides, planetary waves, and gravity waves. Atmospheric thermal tides generated in the lower atmosphere from latent heat release and ozone and water vapor heating attain large amplitudes in the mesosphere and lower thermosphere (MLT) and ionospheric E region, and decay at higher altitudes due to molecular dissipation. In the thermosphere and ionospheric F region, the thermal tides due to solar EUV heating dominate. The tidal winds can strongly affect the E region dynamo [e.g., *Richmond*,

[1]High Altitude Observatory, National Center for Atmospheric Research, Boulder, Colorado, USA.

0148-0227/10/2009JA015188

1983]. Recent observations have shown longitudinal variations of F region electron density with wave number 4 [*Immel et al.*, 2006], which is thought to be a signature of the diurnal, eastward propagating wave number 3 nonmigrating tide [*Hagan et al.*, 2009]. Numerical simulations suggest that ultrafast Kelvin waves and short-period planetary waves can propagate up to 150 km and capable of causing ionospheric perturbations, while long-period and quasi-stationary planetary waves cannot penetrate to the thermosphere [*Forbes*, 2000; *Takahashi et al.*, 2007; *Pogoreltsev et al.*, 2007]. *Pogoreltsev et al.* [2007] concluded that nonmigrating tides generated from tidal and planetary wave interaction could play an important role in the lower and upper atmosphere coupling.

[4] The role of planetary waves (PWs) in the ionospheric day-to-day variability is not very clear. On the one hand, even though planetary waves can propagate up to the mesosphere and may even amplify due to instability [*Plumb*, 1983; *Meyer and Forbes*, 1997; *Liu et al.*, 2004], further upward propagation of planetary waves is limited by the increasingly strong molecular dissipation and filtering by critical layers due to wind reversal in the MLT. On the other hand, the ionospheric variability often displays planetary wave periods (e.g., quasi 2 day, 5–7 day, 9–15 day, etc.) [*Laštovička and Pancheva*, 1991; *Chen*, 1992; *Altadill and Apostolov*, 2001; *Xiong et al.*, 2006]. It is difficult, however, to clearly separate the impacts by the traveling planetary waves from those coming from geomagnetic disturbances on the ionospheric day-to-day variability [*Xiong et al.*, 2006].

[5] The level of geomagnetic activity has been very low since 2008 because of the extreme solar minimum. Facilitated by this low geomagnetic activity, recent studies have clearly identified the large perturbations of ion temperature, ion drift, and total electron density during stratospheric sudden warming (SSW) events [*Goncharenko and Zhang*, 2008; *Chau et al.*, 2009]. Because an SSW is caused by the rapid growth of quasi-stationary planetary waves (QSPW) [*Matsuno*, 1971], the observed ionospheric variability could be related to these waves. In this work, we will study the impact of a QSPW on the ionosphere under solar minimum and geomagnetic quiet conditions. Apart from being the main driving force of an SSW, QSPWs are a universal dynamical feature in the winter middle atmosphere and they generally have amplitudes larger than traveling planetary waves (e.g., quasi 2 day wave, 5–7 day waves). Their propagation into the middle atmosphere is closely related to the tropopause wind: they are blocked by the zero wind line at the tropopause during summer and start to propagate into the stratosphere and mesosphere when this zero wind line begins to disappear. According to *Charney and Drazin* [1961], only the QSPWs with small wave numbers (large wavelengths) can propagate into the middle atmosphere, while components with large wave numbers are trapped in the troposphere. It is also found in previous studies that QSPWs can nonlinearly interact with atmospheric tides, leading to global responses of both migrating and nonmigrating components [e.g., *Hagan and Roble*, 2001; *Liu et al.*, 2007; *Fuller-Rowell et al.*, 2008; *Chang et al.*, 2009]. The interactions between planetary waves and tides are likely responsible for the most significant nonmigrating tides in the lower thermosphere and ionosphere E region: the zonally symmetric diurnal tide, the eastward propagating diurnal and semidiurnal tides with zonal wave numbers 2 and 3, the westward propagating diurnal wave number 2, semidiurnal wave numbers 1, 3, and 4, and terdiurnal wave number 5 identified from the analysis of temperature measurements by the Sounding of the Atmosphere using Broadband Emission Radiometry (SABER) instrument on board of the Thermosphere Ionosphere Mesosphere Energetics and Dynamics (TIMED) satellite [*Forbes et al.*, 2008]. In this study, we will examine how the ionosphere is affected by the interaction between a QSPW and migrating tides.

[6] A description of the numerical model used for this study and the numerical experiments is given in the next section. Analysis of the model results is then presented in section 3. Section 4 discusses the relevance of these results as related to previous observations. Conclusions are given in section 5.

2. NCAR TIME-GCM

[7] For this study, the NCAR thermosphere-ionosphere-mesosphere electrodynamics general circulation model (TIME-GCM) is used. The NCAR TIME-GCM is a time-dependent, three-dimensional model that solves the fully coupled, nonlinear, hydrodynamic, thermodynamic, and continuity equations of the neutral gas self-consistently with the ion energy, ion momentum, and ion continuity equations from the upper stratosphere to the thermosphere. It combines all previous features of the NCAR thermosphere and ionosphere GCMs, including the self-consistent, fully coupled thermosphere and ionosphere, and electrodynamics driven by the neutral wind circulation [*Roble et al.*, 1988; *Richmond et al.*, 1992; *Roble and Ridley*, 1994]. The TIME-GCM predicts global winds, temperatures, major and minor species composition, electron and ion densities and temperatures, and the ionospheric dynamo electric field. The regular horizontal resolution of the TIME-GCM is 5° × 5°, and the upper boundary of the model for this study is set at 4.6×10^{-10} hPa, two scale heights higher than the usual upper boundary of the TIME-GCM. For solar minimum conditions, this corresponds to an increase from ~390 km to ~480 km. There are 49 pressure surfaces from 10 hPa (30 km height) to the upper boundary with a vertical resolution of one-half scale height. The input parameters for the TIME-GCM are solar EUV and UV spectral fluxes, parameterized by the F10.7 cm solar flux index, auroral particle precipitation, an imposed magnetospheric electric field, and the amplitudes and phases of migrating tides from the lower atmosphere specified by the Global Scale Wave Model (GSWM) [*Hagan et al.*, 1999]. The gravity wave effects are parameterized based on the linear saturation theory of *Lindzen* [1981]. The details of the model and comparison of model results with observations are given by *Roble* [2000, and references therein].

[8] For this study, the lower boundary conditions are specified without and with a QSPW perturbation. The base case without QSPW is a climatological simulation for the period of January–March, and the only planetary scale perturbations specified at the lower boundary of the model are migrating tides from GSWM. In the control case, an idealized QSPW with zonal wave number 1 is specified at the lower boundary through geopotential height perturbation in addition to the tides. This simulation starts on day 15, and the amplitude of the QSPW is ramped up using a gaussian function with an e-folding time of 7 days and peak time on

day 30. The wave amplitude is kept at the peak value for 10 days before being ramped down using the gaussian function. The amplitude of the wave is specified over northern latitudes, peaking at 60°N with the maximum value of 2500 m (day 30–40). This is somewhat larger compared with climatological wave amplitudes at this altitude. The reason for using this large wave amplitude is to counter the unrealistic decay of the forced waves near the lower boundary in TIME-GCM. The F10.7cm radio flux is set at 70, and the geomagnetic activity is low with the hemispheric power, cross-tail potential and B_z set to 10 GW, 30 kV and 0, respectively.

3. Analysis

3.1. Interaction Between Planetary Wave and Tides

[9] As found in previous studies, PWs can cause variability of migrating and nonmigrating tides through nonlinear interactions. This is demonstrated here in Figure 1 for the specific cases in this study, which shows the two dimensional (longitude and time) fast Fourier transform (FFT) analysis of the difference in the meridional wind between the cases with and without the QSPW. The difference is calculated by subtracting the meridional wind without QSPW from that with QSPW. The FFT here is performed over 24 h on day 31, when the vertical drift display large changes as will be seen later. As seen from Figure 1a, the QSPW component is mostly confined to the high latitudes and below the lower thermosphere. The QSPW component above 100 km in the northern hemisphere is from in situ generation by filtered gravity waves [*Smith*, 1996], and that at high southern latitudes is probably from the secondary interaction between the migrating and nonmigrating tides. This component thus cannot cause significant ionospheric changes at low latitudes. On the other hand, migrating (Figures 1b and 1c) and nonmigrating tides (Figures 1d–1f) experience significant changes at extended latitudes and altitudes as a result of the nonlinear interaction with QSPW: The migrating diurnal tide, migrating semidiurnal tide, and the nonmigrating semidiurnal westward propagating wave number 1 shows changes larger than 20 m s^{-1}, and all tidal components shown here have changes larger than 10 m s^{-1} at low or midlatitudes. The changes of these tidal components are largest between 100–150 km (E region), and extend into the upper thermosphere and the ionosphere F region. These tidal components can thus affect the entire thermosphere and ionosphere.

3.2. Changes of the Ion Drift

[10] The zonal electric field and the vertical ion drift change significantly when the QSPW is introduced. Figure 2a compares the vertical ion drift at 7.5°N and 70°W from simulations without and with the QSPW. The vertical ion drifts from the two cases start to show considerable differences between day 20–25, and the differences show a clear diurnal and semidiurnal pattern (Figure 2b). At this longitude, the largest difference in vertical ion drift occurs at ~0500 local time (LT). Starting from about day 25 the vertical ion drift around 0500 LT changes from weakly downward to upward, and the magnitude of the upward drift increases steadily till day 31. Afterward the magnitude of the upward drift varies between 10 and 35 m s^{-1}, even though the QSPW amplitude is kept as a constant between days 30–40. From the vertical drift difference (Figure 2b), it is seen that the perturbation at other local times also becomes more irregular after day 31. These results indicate that the ionospheric system does not reach a steady state, probably due to the strong nonlinearity in response to the large QSPW.

[11] Figure 3 shows the vertical ion drifts near the F2 peak at 1000 universal time (UT) on day 31 for the the cases without and with QSPW. The large upward enhancement of the vertical drift is evident around 70°W (0500 LT). It is also clear from the map that this enhancement of the upward drift extends to higher latitudes, with the largest changes between 20–30° geomagnetic latitudes (by about 40 m s^{-1}). The vertical drift also changes at other longitudes/local times. For example, the downward drift between 2200–0300 LT and upward drift around 1600 LT become stronger (also can be seen from the difference of the vertical ion drift in Figure 9). The magnitude of these changes are not as large as that near 0500 LT. A large eastward change of zonal ion drift in F region is seen before dawn (not shown).

[12] The ion drift changes are dependent on time and longitude, as can be seen in Figure 4. In Figure 4, the straight lines mark the phase velocities corresponding to the migrating, semidiurnal westward propagating wave number 1, and diurnal westward propagating wave number 2 tidal components. By comparing the contour lines of the vertical drift difference, it is seen that the difference is a superposition of these components. For example, the downward change of the drift around ~0600 LT between 20°E–120°E and the relatively weak downward change at local noon at longitudes west of 100°E bear a clear migrating tidal signature ($-360°d^{-1}$). The upward change around 0600–0700 LT between 120°W–180°W and 100°E–180°E, and at ~1700 LT between 40°E–120°E also display the same phase velocity. The phase velocity at 1000–1500 UT between 90°W–180°W is $-720°$ d^{-1}, and that between 0000–1200 UT/0–80°W and 1700–2400 UT/60°E–0°E is $-180°$ d^{-1}. They correspond to semidiurnal westward propagating wave number 1 and diurnal westward propagating wave number 2 nonmigrating components, respectively. Superposition of these three components is visible between 0600–1200 UT and 0–80°W, and the largest upward change of the vertical drift (~40 m s^{-1}) occurs within this time period and longitude sector (between 0400–0500 LT and 60–70°W). These general features are similar but the specific details vary significantly from day to day. These results suggest that the QSPW can strongly affect the ionospheric drift through modulating migrating and nonmigrating tides, consistent with the spectral analysis in section 3.1.

[13] The perturbations due to both migrating and nonmigrating tides introduce complex spatial and temporal variability, which makes it challenging to interpret observations. For example, the local time behavior of the vertical ion drift perturbation is very different at different longitudes, as seen in Figure 5. At 70°W, the vertical ion drift changes sign and becomes strongly upward before sunrise (~0500 LT), while at the same local time at 70°E the downward vertical drift is significantly enhanced. At 15°E, on the other hand, the vertical drift perturbation is relatively small at all local times. An important implication of this longitude and local time dependence of the ionospheric variability is that

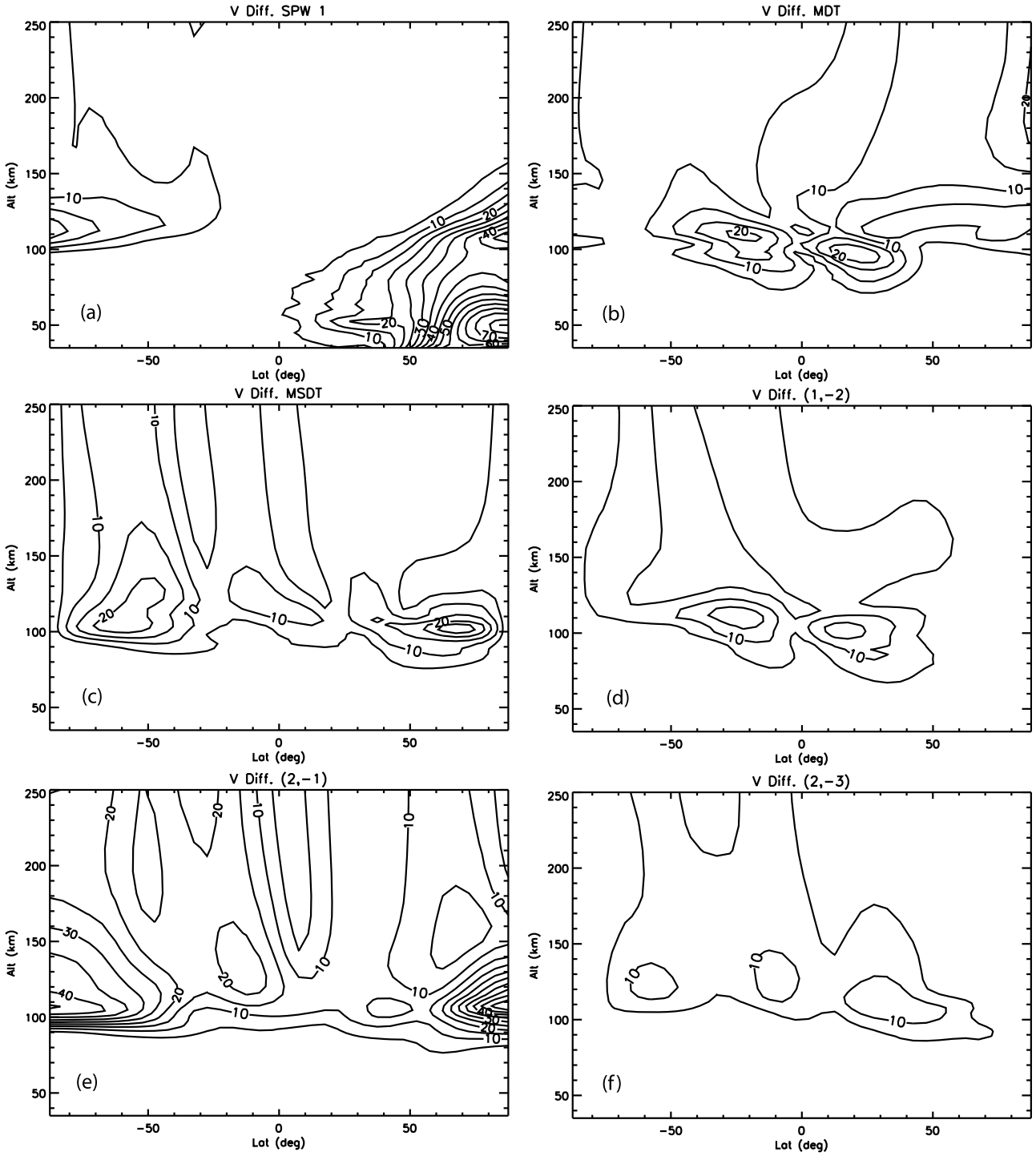

Figure 1. Spectral amplitude of the difference in the meridional wind between the cases with and without the quasi-stationary planetary wave. (a) Stationary planetary wave with wave number 1, (b) diurnal migrating component, (c) semidiurnal migrating component, (d) diurnal westward propagating wave number 2, (e) semidiurnal westward propagating wave number 1, and (f) semidiurnal westward propagating wave number 3. Contour interval is 5 m s^{-1}.

global information, either from satellite or network of ground-based measurements, is necessary to correctly interpret such variability.

[14] The specific structures of the variability are sensitive to the phase of the QSPW and the interacting tides. A TIME-GCM numerical experiment is done with the phase of the stationary QSPW specified at the lower boundary shifted by 180° in longitude. From Figure 6, it is seen that the pattern of the changes in the vertical drift are shifted by 180° compared with Figure 4 (for the same local time). The knowledge of the

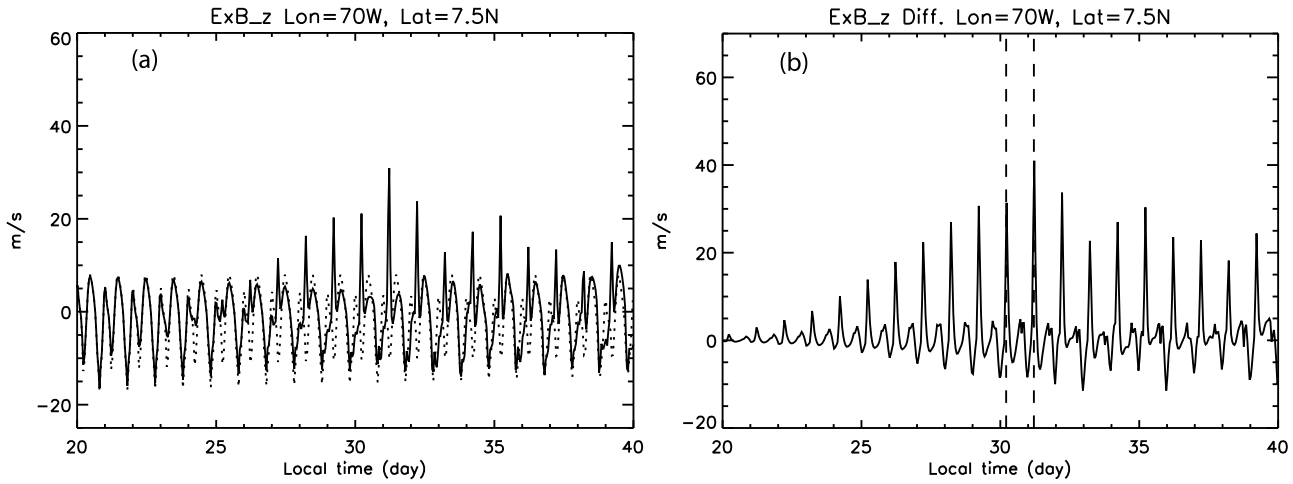

Figure 2. (a) Vertical component of the F region ion drift at 7.5°N and 70°W from the cases without (dotted line) and with (solid line) QSPW. (b) The difference between the two drift velocities in Figure 2a. The dashed lines in Figure 2b indicate 0500 LT for days 30 and 31.

QSPW is thus critical for the correct modeling and interpretation of the ion drift perturbations.

[15] The perturbation in the vertical ion drift can result from changes of the neutral winds in the dynamo region. To better determine the wind dynamo effects, additional numerical experiments are conducted. These numerical experiments are based on the case with QSPW specified at the lower boundary. In these numerical experiments, the neutral zonal wind, meridional wind, or both are replaced by those from the base case simulation at corresponding times in either the E region (100–150 km) or the F region (155–500 km) in the dynamo module. The numerical model is integrated only one time step, so that there is no feedback interaction between the dynamo and the neutral winds. We should also emphasize that the neutral winds are only replaced in the dynamo calculation, and thus the neutral dynamics is not affected. By comparing these model results with the original case with QSPW, we can determine the relative contribution to the perturbation in vertical ion drift from neutral winds in the E and F regions. Figure 7 shows the vertical ion drifts at 2.5°N (geographic) from these numerical experiments. In Figure 7a, at ~0500 LT the upward vertical ion drift decreases from 25 m s^{-1} to 7 m s^{-1} and 3 m s^{-1} when the neutral meridional wind and zonal wind are replaced, respectively. It becomes downward if both winds are set to the base case. The results thus suggest the both zonal and meridional winds in the E region contribute to the enhancement of the upward ion drift at 0500 LT. On the other hand, replacing the winds in the F region does not seem to significantly change the enhancement of the vertical ion drift (Figure 7b), and the upward vertical drift perturbation at ~0500 LT actually slightly increases when the F region neutral winds are replaced. Therefore, these numerical experiments suggest that the QSPW-tidal interaction alter the vertical ion drift at dawn mainly through E region wind dynamo. This conclusion, we want to emphasize, is obtained for solar minimum conditions

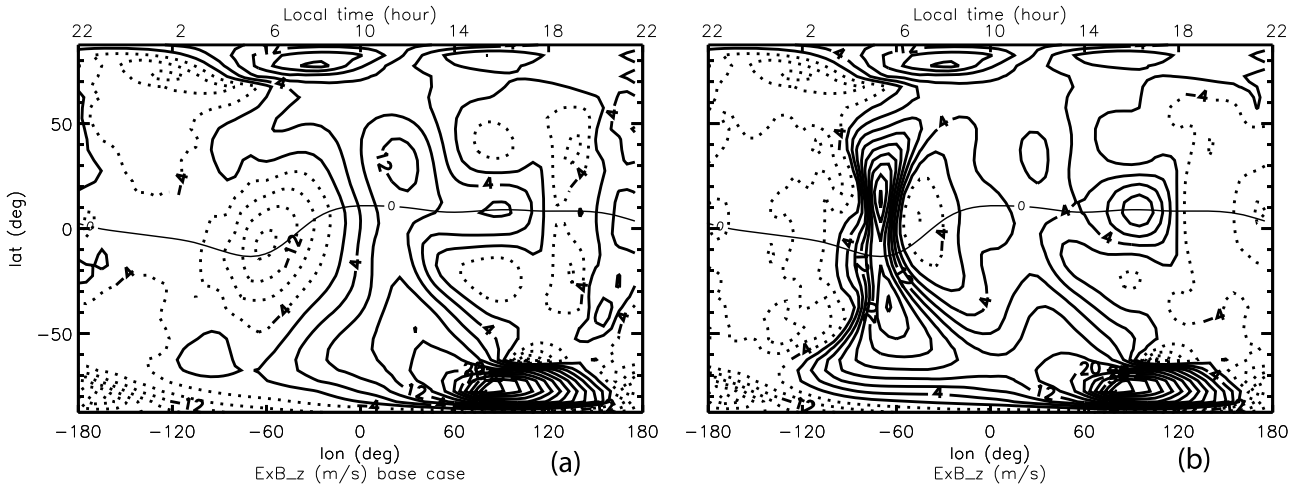

Figure 3. F region vertical ion drift at 1000 UT, day 31 from (a) the case without QSPW and (b) the case with QSPW. Contour intervals are 4 m s^{-1} (solid is for upward). The geomagnetic equator is shown by the thin solid line.

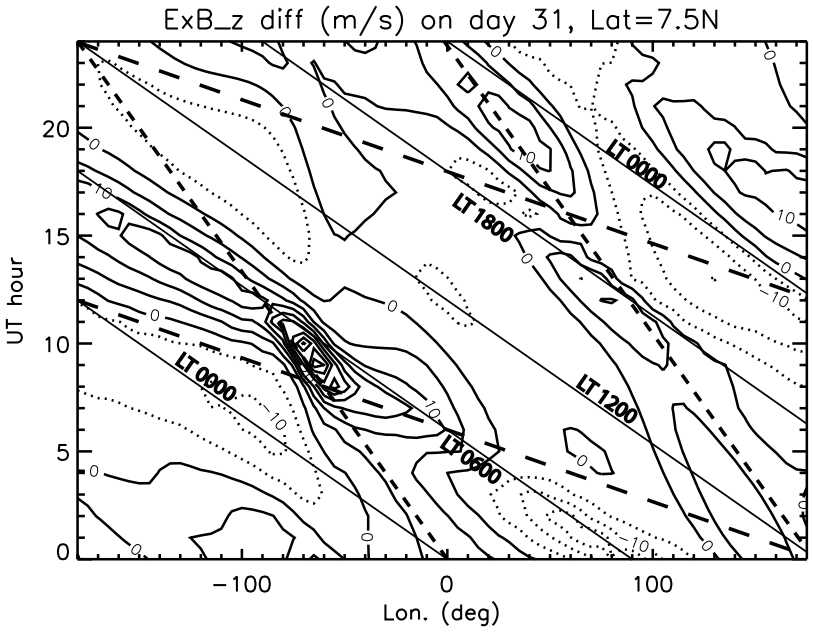

Figure 4. The difference of the vertical ion drift at 7.5°N on day 31 between the cases with and without QSPW. Contour interval is 5 m s^{-1}. Solid is for upward. The straight lines denote the phase velocities of migrating component (solid), diurnal westward propagating wave number 2 (short-dashed line), and semidiurnal westward propagating wave number 1 (long-dashed line) components. The local times are marked on each of the solid phase lines.

when the F region Pedersen conductivity is relatively small. For solar maximum conditions the F region conductivity is much larger than at solar minimum [e.g., *Takeda and Araki*, 1985], and F region dynamo effects will be relatively much more important than for the present simulations. The dependence of the ionospheric response on the solar activity will be presented in a future study.

[16] The change of the E region neutral winds when the QSPW is specified are then examined in Figure 8, because of their important role in this process. The pressure level chosen here is 2.1×10^{-5} hPa (~120 km), where the Hall conductivity is at or near its maximum in the early morning and the Pedersen conductivity also becomes quite large (near its E region peak at ~130 km). From Figure 8, it is seen that the positive zonal gradients of the zonal wind change are large around 70°W (and 0500 LT) south of the dip equator, and that the positive (negative) zonal gradients of the meridional wind are large ~20° south (north) of the dip equator at the same location and local time. The zonal and meridional winds contribute to the total zonal current through wind-driven Hall and Pedersen currents, $J_x^{W,H}$ and $J_x^{W,P}$, respectively:

$$J_x^{W,H} = \sigma_H u B \tag{1}$$

$$J_x^{W,P} = -\sigma_P v B \sin I \tag{2}$$

where σ_H and σ_P are the Hall and Pedersen conductivities, u and v the neutral zonal and meridional winds, B geomagnetic field, I the downward magnetic inclination, and x denotes the zonal direction. (The distinction between geographic and geomagnetic directions is ignored here.) Therefore, the convergence of the wind-driven zonal current $-\partial(J_x^{W,H} + J_x^{W,P})/\partial x$, which determines the accumulation of polarization charges,

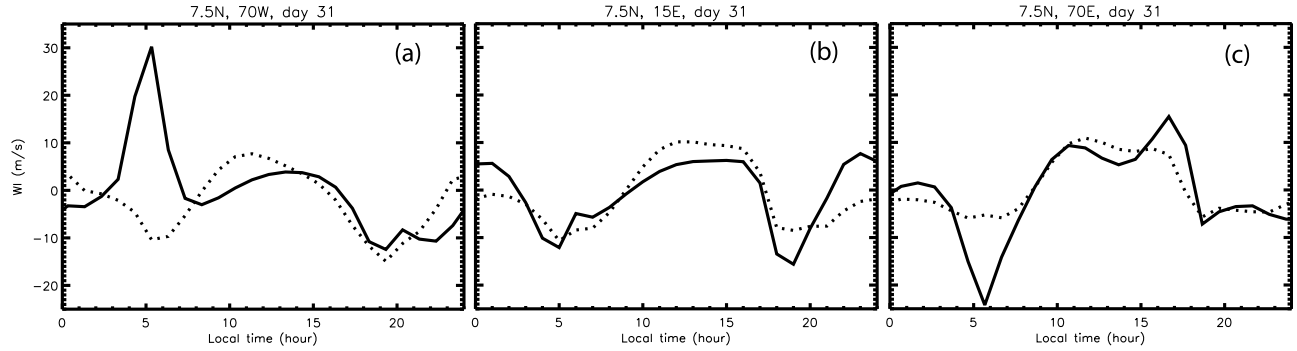

Figure 5. Vertical component of the ion drift at 7.5°N and (a) 70°W, (b) 15°E, and (c) 70°E from the cases without (dotted line) and with (solid line) QSPW.

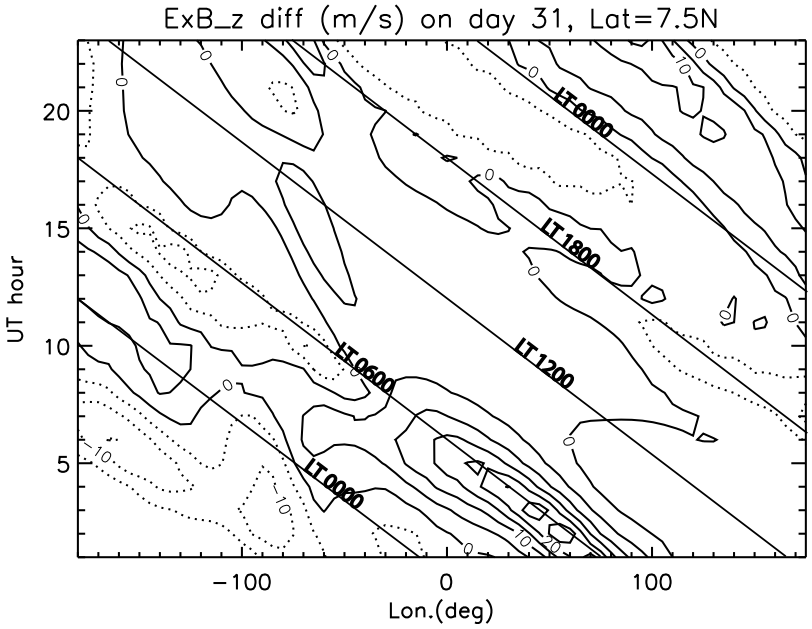

Figure 6. Similar to Figure 4, except that the phase of the specified QSPW in the numerical experiment is shifted by 180° in longitude.

is dependent on the zonal gradients of the winds and the electric conductivities. For example, the large positive zonal gradients in the zonal wind ($\partial u/\partial x > 0$) tend to cause divergence in wind-driven Hall current ($-\partial J_x^{W,H}/\partial x < 0$); and the positive (or negative) zonal gradients of the meridional wind $\partial v/\partial x > 0$ (or $\partial v/\partial x < 0$) south (or north) of the dip equator $I < 0$ (or $I > 0$) result in divergence of the wind-driven Pedersen current ($-\partial J_x^{W,P}/\partial x < 0$). Therefore, zonal gradients of both zonal and meridional winds contribute to the accumulation of negative polarization charges, consistent with our findings from Figure 7a that both wind components contribute to the vertical ion drift change. This is further verified by calculating the difference of $-\partial(J_x^{W,H} + J_x^{W,P})/\partial x$ between the case with and without the QSPW at ~120 km (Figure 9). The current shows a strong divergence, and thus accumulation of negative polarization charge, around 60°W and 0600 LT at low latitudes and midlatitudes in both hemispheres. This in turn results in an eastward polarization electric field and an upward ion drift to the west of this region. To confirm this, we have overplotted the change in vertical drift on the divergence contour and the peak upward drift is indeed located to the west of the region with the

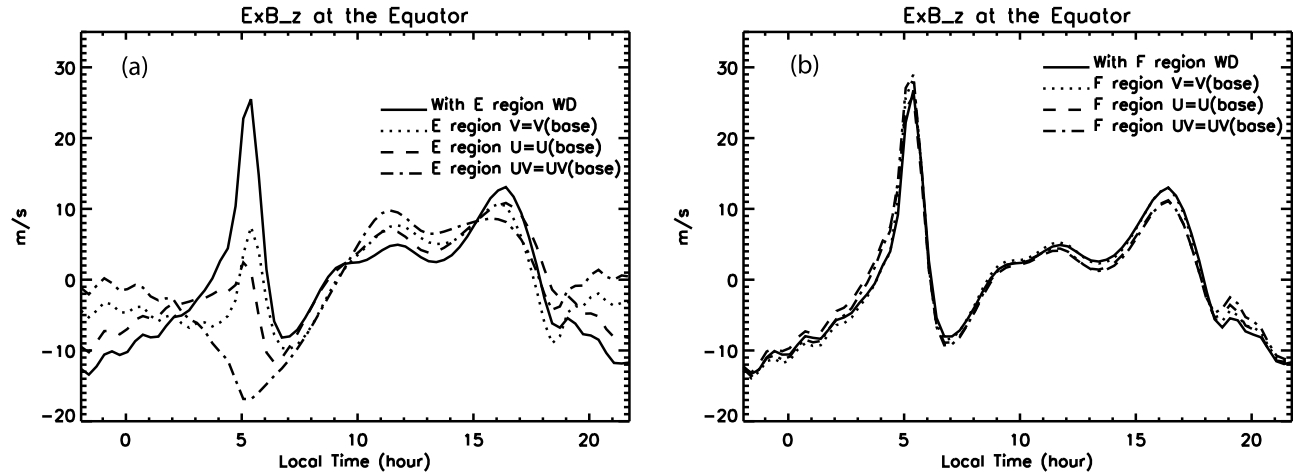

Figure 7. (a) Vertical ion drift of several cases with specified QSPW. Solid line is for the original case with QSPW, dotted line is for the case with specified QSPW but the neutral meridional wind in E region is set to the base case without QSPW when calculating dynamo, dashed line is for the case with specified QSPW but the neutral zonal wind in E region is set to the base case without QSPW when calculating dynamo, and dash-dot line is for the case with specified QSPW but both the neutral zonal and meridional winds in E region are set to the base case without QSPW when calculating dynamo. (b) Similar to Figure 7a but the winds are now set to the base case in F region.

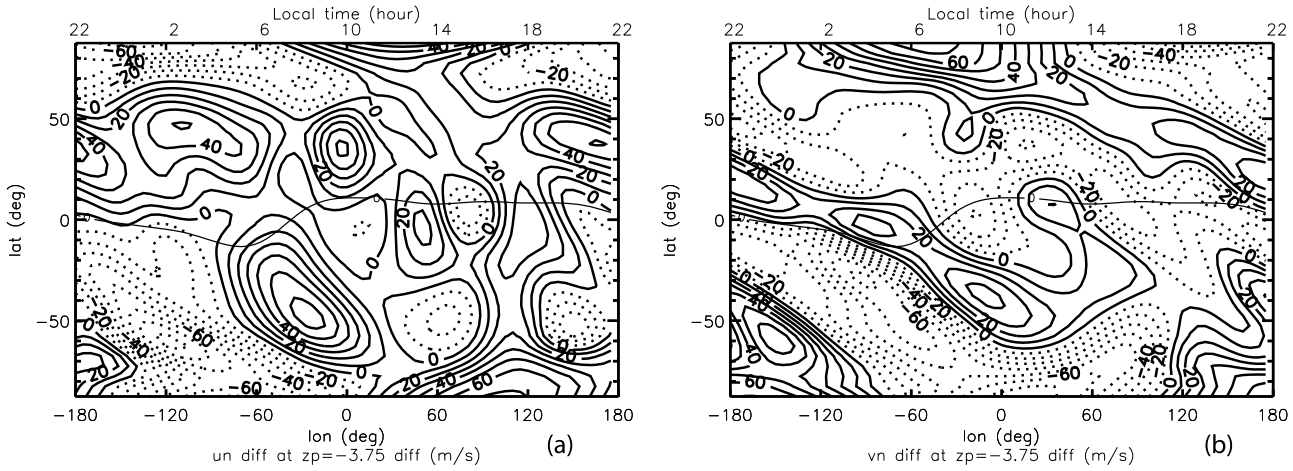

Figure 8. The difference of the (a) zonal and (b) meridional winds at ~120 km and 1000 UT (day 31) between the cases with and without QSPW. Contour interval is 10 m s^{-1}. Solid is for eastward in Figure 8a and northward in Figure 8b.

largest current divergence. It is also seen from Figure 9 that there is no large downward ion drift to the east of the region, probably because the large electric conductivities in the daytime prevent the buildup of large electric potential difference. It should be noted that a comprehensive analysis of the divergence should consider currents in all 3 directions and should be integrated along the field lines. In Figure 9 we have only examined the divergence of zonal current at an E region altitude for simplicity, and also because the E region wind dynamo is most important as shown above, and the zonal current change is most significant across the terminator.

[17] The electric conductivities change rapidly at dawn (Figure 10a), and should also play an important role in the change of polarization electric field according to equations (1) and (2). This is confirmed in a numerical experiment, which makes a one time step integration at 1000 UT on day 31 for the case with QSPW. In this

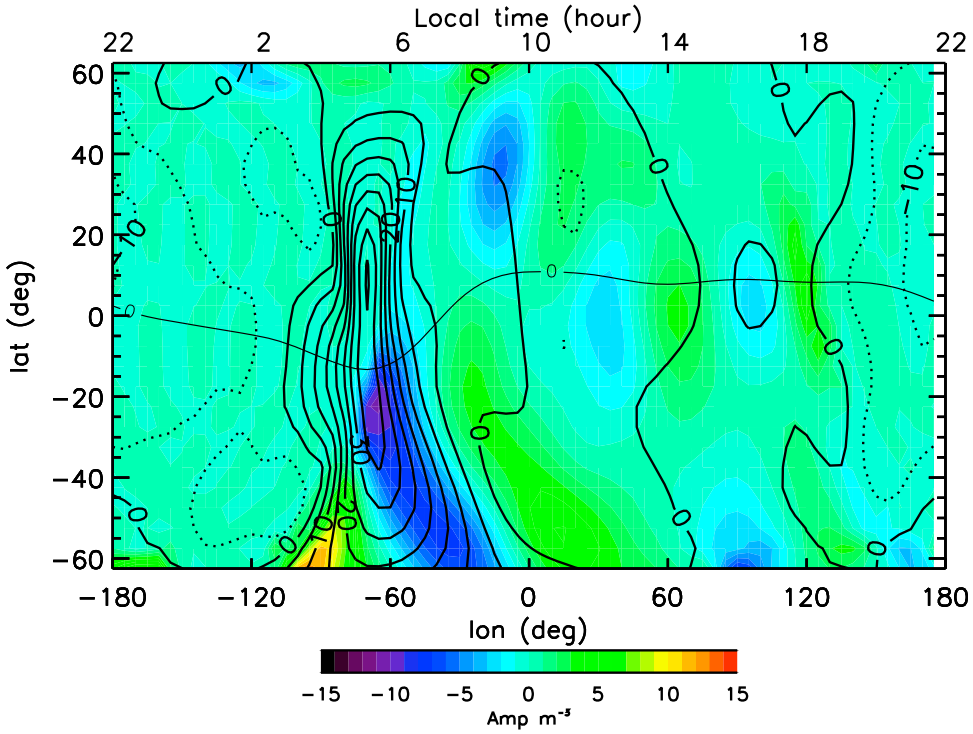

Figure 9. Color contour is the difference of the convergence of the total zonal current between the cases with and without QSPW at an E region height (120 km) and 1000 UT (day 31). Overplotted line contour is for the change in vertical ion drift (contour interval is 5 m s^{-1}, and solid is for upward).

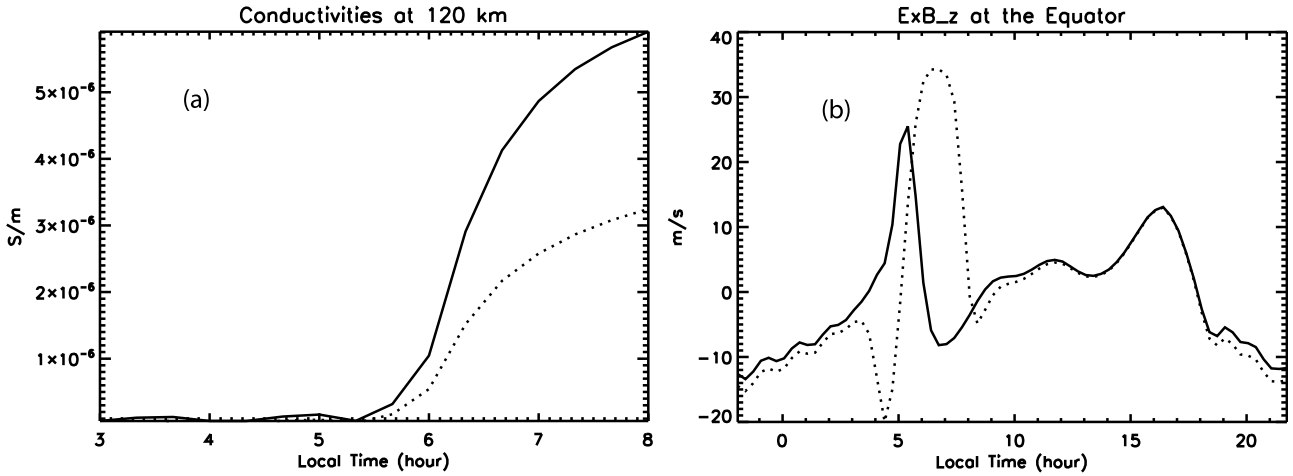

Figure 10. (a) Hall (solid line) and Pedersen (dotted line) conductivities at 1000 UT, 2.5°N, and ~120 km. (b)Vertical ion drift at 1000 UT and 2.5°N from TIME-GCM simulations with QSPW. Solid line is the original simulation, and dotted line is the simulation with the zonal gradient of both conductivities set to 0 between 0400 and 0800 LT in the E region (see text for explanation).

numerical experiment, the Hall and Pedersen conductivities in the E region (100–150 km) between 90°W–30°W (corresponding to 0400–0800 LT) are set to be equal to the values at 90°W so that the zonal gradients of the conductivities are 0 within this longitude range. As seen from Figure 10b, the enhancement of the upward ion drift disappears around 75°W (0500 LT) and its peak shifts to 45°W (0700 LT), close to the discontinuity in the electric conductivities at 30°W (0800 LT).

[18] Figure 11 shows the E region neutral winds change at 17.5°S between 0000 and 2300 UT on day 31. Like the change of the vertical drift (Figure 4), the changes in the winds are also a superposition of migrating and nonmigrating tides and are thus both longitude and local time dependent. The zonal gradients of both wind perturbations between ~0–100°W and ~0500–1000 UT are large, and contribute to the zonal current divergence in a constructive way. However, the phases of the zonal and meridional winds are not always the same, so that their contribution may not be constructive at other local times and locations. The combination of the variety of wave components and different phases of zonal and meridional winds introduces complexity to the changes of spatial and temporal structures of ionosphere perturbations.

3.3. Changes of the F2 Region Electron Densities

[19] The variability of the vertical ion drift due to QSPW and tidal interaction redistributes ionospheric ions and electrons. Figure 12 shows the differences of the F2 peak height, the F2 peak electron density and the total electron contents (TEC) at 70°W on day 31, between the cases with and without the QSPW. Around dawn, the F2 peak electron density decreases and its height increases around the equator, corresponding to the large upward drift in the presence of the QSPW. The largest F2 peak height increase is more than

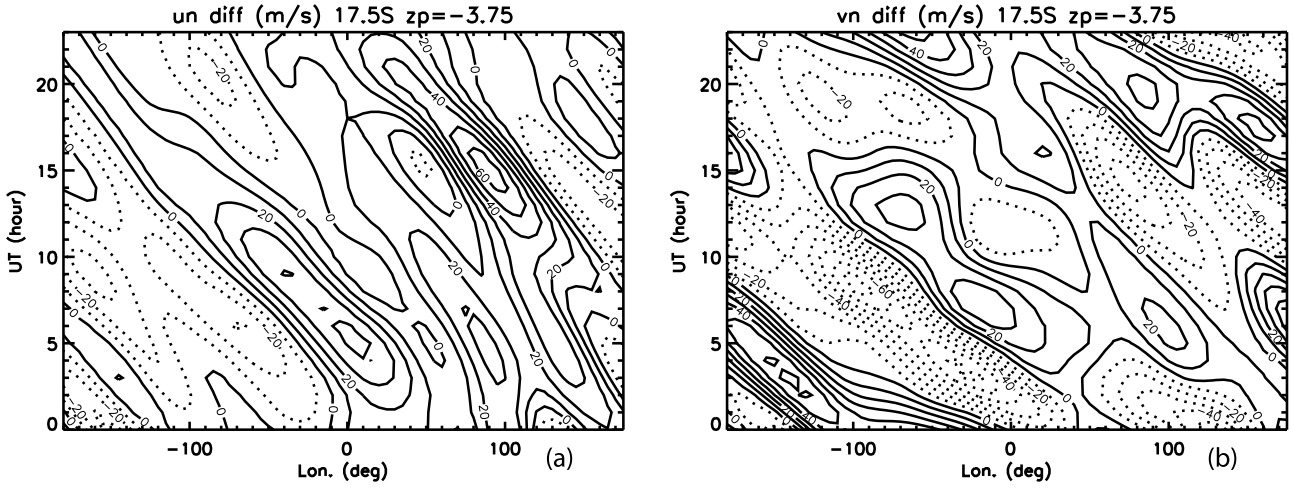

Figure 11. The difference of the (a) zonal and (b) meridional winds at 17.5°S on day 31 between the cases with and without QSPW. Contour interval is 10 m s^{-1}. Solid is eastward in Figure 11a and northward in Figure 11b.

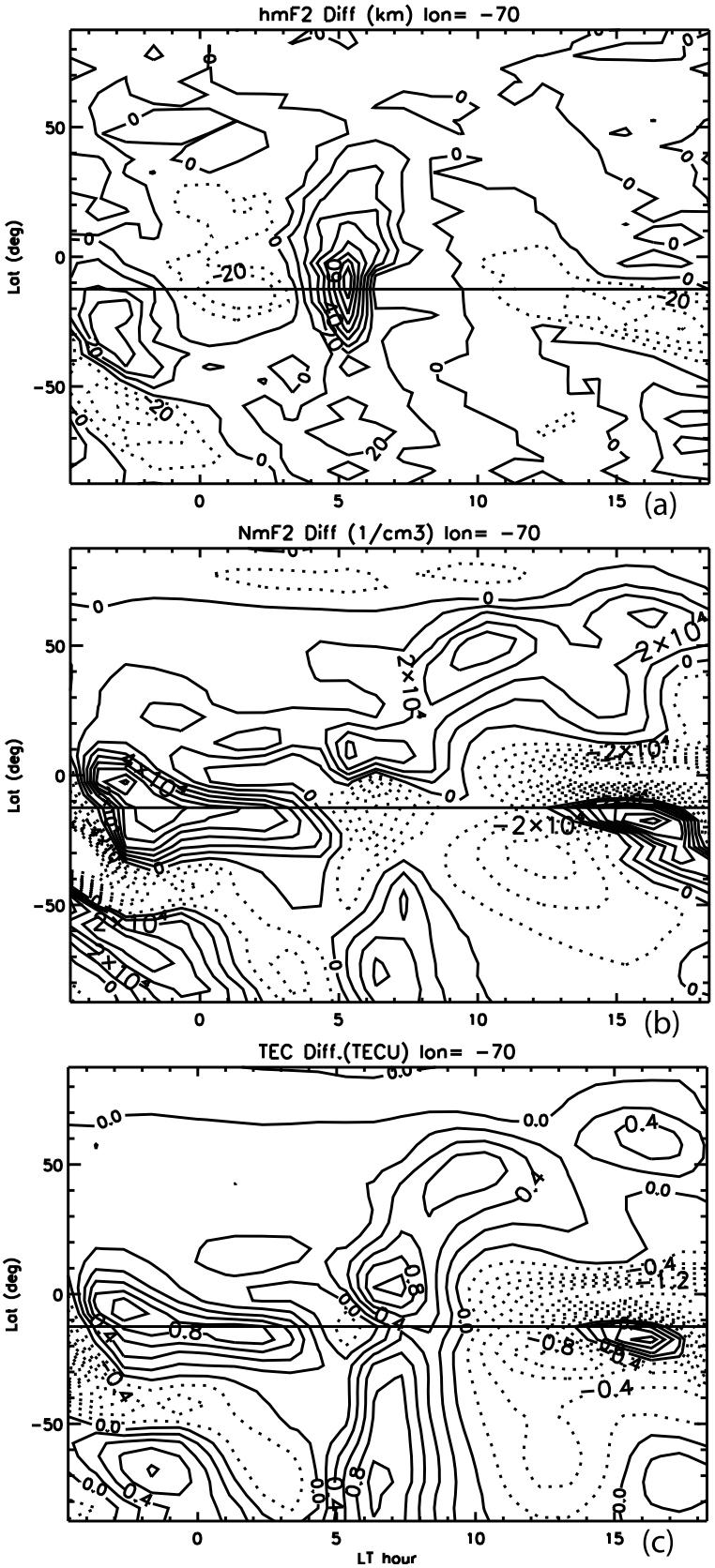

Figure 12. The difference of the (a) F2 peak height, (b) F2 peak electron density, and (c) total electron content (TEC) at 70°W on day 31 between the cases with and without QSPW. Contour intervals are 10 km (Figure 12a), 10^4 cm^{-3} (Figure 12b), and 0.2 TEC unit (Figure 12c). Solid contour lines denote increase of the respective quantities.

80 km, occurring shortly after 0500 LT and close to the dip equator. This upward vertical drift redistributes the ion and electron density along the field lines to higher latitudes, and enhances the Appleton anomaly. As a result, the F2 peak density near the dip equator decreases while that further poleward increases. The TEC at the dip equator also decreases between 0400–0600 LT and increases at higher latitudes. The F2 peak density and TEC increases last till ~1000 LT, with the largest increases occurring about an hour after the maximum upward drift. Prior to the upward drift at 0500 LT, the F2 peak density and TEC increase near the dip equator and decrease poleward in the southern hemisphere. This is probably because the enhanced downward transport at the equator causes the convergence of ions/electrons from higher latitudes. It should be noted that the changes in electron density and TEC are also related to field-aligned transport by F region neutral wind, as well as photochemical processes. These processes will be analyzed in more detail in future studies.

4. Discussion

[20] Large ionospheric variations at low latitudes around dawn have been observed for geomagnetically quiet periods. As reported by *Chau et al.* [2009], the vertical ion drift velocity over Jicamarca (11.95°S geographic, 1.5°S geomagnetic, 77°W) is usually weak at 0600–0700 LT (magnitude less than 10 m s^{-1}), but becomes strongly upward (exceeding 60 m s^{-1}) between 22 and 26 January 2008. This change is consistent with the vertical ion drift changes seen in the model simulation (Figure 2). *Chau et al.* [2009] pointed out that this change coincides with a stratospheric sudden warming event. Because the stratospheric sudden warming is caused by the increase of QSPWs and their interaction with the stratospheric mean circulation, the observed change of vertical drift may be interpreted as a result of planetary wave and tidal interaction as revealed by the numerical experiments in this study. It is also found that the difference between the ion temperature observed above Millstone Hill (42.6°N geographic, 55°N geomagnetic, 71.5°W) in January 2008 (with a strong SSW) and that observed in January 2007 (no SSW) has a strong semidiurnal period above 200 km [*Goncharenko and Zhang*, 2008]. This may be interpreted as changes caused by strong nonmigrating semidiurnal tide. The nonmigrating semidiurnal tide is generated by the nonlinear interaction between the QSPW and the migrating semidiurnal tide, as discussed in section 3.1. Compared with the observed change in TEC [*Goncharenko et al.*, 2010, also manuscript in preparation, 2010], the TEC change from the model (Figure 12c) is smaller. This may be caused by the somewhat artificial boundary condition imposed on the ion and electron fluxes at the upper boundary. The specified upper boundary plasma flux in the model does not depend on changes in vertical drift velocities, which inhibits changes in high-altitude plasma transport associated with the equatorial plasma fountain.

[21] The changes of the vertical drift around dawn can also be downward. *Nayar et al.* [2009] showed a case where the vertical drift becomes strongly downward (≈60 m s^{-1}) at 0630 LT over Trivandrum (8.3°N geographic, 0.4°N geomagnetic, 77°E) on 23 December 2004. This behavior is qualitatively similar to the vertical drift from the model at a similar location (Figure 5c). As explained in section 3.2, the longitude/local time dependence is determined by the phase of the QSPW and the tides. Therefore, a quantitative understanding of planetary waves and tides is indispensable for the correct interpretation of variation of the ion drift/dynamo electric field.

[22] The QSPWs are present most of the time in the winter hemisphere and are highly variable. The occurrence of SSW is directly related to the strength of QSPWs, and also depends on other atmospheric conditions, such as the phase of the quasi-biennial oscillation [*Holton and Tan*, 1980] and El Niño and Southern Oscillation [*Sassi et al.*, 2004]. If the interaction between QSPWs and tides is a main cause of ionospheric variability, then such variability may not be limited to major SSW periods. We have performed TIME-GCM simulations similar to those presented in this paper, but with smaller amplitude. Although the magnitude is smaller, the general behavior of the ionospheric variability is similar to what has been presented here. It is thus worth studying the ionospheric responses to QSPWs, including periods with no SSW or only minor SSW. For example, it is known major SSWs are very rare for southern winter (the only one on record is 2002), but the QSPWs may still be strong enough to impact the upper atmosphere. This will be important for understanding large ionospheric disturbances, such as that observed in June 2008 by C/NOFS [*de La Beaujardière et al.*, 2009].

[23] This study focuses on the interaction of QSPW with migrating tides due to solar heating. Lunar tides, whose semidiurnal component is shown to cause enhanced variability during stratospheric sudden warming in a recent study by *Fejer et al.* [2010], are not included in these simulations. Furthermore, the traveling planetary waves (e.g., quasi 2 day wave, 6.5 day wave, fast Kelvin waves) can become large in the MLT region, and contribute to the ionospheric variability either directly or through interaction with tides. The presence of nonmigrating tides (e.g., the diurnal eastward propagating wave number 3 tide) is not considered in the current numerical study, but could be another important factor in ionospheric variability. These are worth further investigation in future research.

5. Conclusions

[24] It is demonstrated through numerical experiments using NCAR TIME-GCM simulations that the presence of a quasi-stationary planetary wave can cause large ionospheric changes, including changes in the dynamo electric field/ion drift, F2 peak height and electron density, and TEC for solar minimum conditions. However, the QSPWs are mostly confined to the winter hemisphere at high latitudes below the mesopause (Figure 1) due to their interaction with critical layers (zero zonal wind for the QSPWs) and the increasing molecular dissipation. They are not likely to directly impact the ionosphere E or F region at equatorial latitudes. Analysis of the simulation shows that the QSPW can nonlinearly interact with tides. Due to the global nature of the tides, the change of both migrating and nonmigrating tides resulting from the nonlinear interaction is not confined, and is actually the largest at low latitudes and in the ionospheric E region. Controlled numerical experiments reveal that large changes in zonal gradients of the zonal and meridional wind in the E region, along with large zonal gradient of electric conduc-

tivities at dawn, can produce large convergence/divergence of Hall and Pedersen currents and thus change the polarization electric field and ion drift. It should be noted that these results are obtained for solar minimum conditions. The dependence of the ionospheric response on the solar activity and the F region conductivity will be studied in future research. The neutral winds in the F region can change quite significantly due to PW and tide interactions (up to 50 m s^{-1}) in the numerical experiments. Their contribution to ionospheric variability also needs to be studied in more detail in future research.

[25] The changes in ion drift are dependent on the longitude and local time. In the numerical experiments, the largest upward change of ion drift occurs near dawn (~0500 LT) around 70°W, and the largest downward change at the same local time around 70°E. There are also longitudes where the ion drift does not change much at the same local time. This complex spatio-temporal pattern is probably related to both the gradient of electric conductivity at dawn and the superposition of the various tidal components. Therefore, quantitative knowledge of the tides and planetary waves is important for the correct interpretation of the observed ionospheric variability.

[26] The numerical results may help us better understand recently observed ionospheric changes during stratospheric sudden warming, when the QSPWs become large. Large upward ion drift has been observed consistently near dawn over Jicamarca on consecutive days during the SSW event in late January 2008 [*Chau et al.*, 2009]. For the same period of time, the ion temperature over Millstone Hill Observatory displays a strong semidiurnal oscillation [*Goncharenko and Zhang*, 2008]. These observed changes in ion drift and semidiurnal tide are consistent with the model results. This suggests that the same underlying mechanism, namely the interaction of planetary waves and tides, could be the cause of the observed changes. The favorable comparison between the observations and the idealized simulation results warrants further research to investigate ionospheric impacts by planetary waves, including QSPWs at nonwarming periods, traveling planetary waves, and fast Kelvin waves. More realistic nonmigrating tides should also be included in future research.

[27] **Acknowledgments.** This work is in part supported by the Office of Naval Research (N00014-07-C-0209), National Science Foundation grants ATM-0535466 and ATM-0836386, and NASA LWS NNX08AQ91G. The National Center for Atmospheric Research is sponsored by the National Science Foundation.

[28] Robert Lysak thanks Tzu-Wei Fang and another reviewer for their assistance in evaluating this paper.

References

Altadill, D., and E. M. Apostolov (2001), Vertical propagating signatures of wave-type oscillations (2 and 6.5 days) in the ionosphere obtained from electron-density profiles, *J. Atmos. Terr. Phys.*, *63*, 823–834.

Altadill, D., and E. M. Apostolov (2003), Time and scale size of planetary wave signatures in the ionospheric F region, role of the geomagnetic activity and mesosphere/lower thermosphere winds, *J. Geophys. Res.*, *108*(A11), 1403, doi:10.1029/2003JA010015.

Chang, L. C., S. E. Palo, and H.-L. Liu (2009), Short-term variation of the s = 1 nonmigrating semidiurnal tide during the 2002 sudden stratospheric warming, *J. Geophys. Res.*, *114*, D03109, doi:10.1029/2008JD010886.

Charney, J. G., and P. G. Drazin (1961), Propagation of planetary scale disturbances from the lower to the upper atmosphere, *J. Geophys. Res.*, *66*, 83–109.

Chau, J. L., B. G. Fejer, and L. P. Goncharenko (2009), Quiet variability of equatorial ExB drifts during sudden stratospheric warming event, *Geophys. Res. Lett.*, *36*, L05101, doi:10.1029/2008GL036785.

Chen, P.-R. (1992), Two-day oscillation of the equatorial ionization anomaly, *J. Geophys. Res.*, *97*, 6343–6357.

de La Beaujardière, O., et al. (2009), C/NOFS observations of deep plasma depletions at dawn, *Geophys. Res. Lett.*, *36*, L00C06, doi:10.1029/2009GL038884.

Fejer, B. G., M. E. Olson, J. L. Chau, C. Stolle, H. Lühr, L. P. Goncharenko, K. Yumoto, and T. Nagatsuma (2010), Lunar dependent equatorial ionospheric electrodynamic effects during sudden stratospheric warmings, *J. Geophys. Res.*, doi:10.1029/2010JA015273, in press.

Forbes, J. M. (2000), Wave coupling between the lower and upper atmosphere: Case study of an ultra-fast Kelvin wave, *J. Atmos. Sol. Terr. Phys.*, *62*, 1603–1621.

Forbes, J. M., S. Palo, and X. Zhang (2000), Variability of the ionosphere, *J. Atmos. Sol. Terr. Phys.*, *62*, 685–693.

Forbes, J. M., X. Zhang, S. Palo, J. Russell, C. J. Mertens, and M. Mlynczak (2008), Tidal variability in the ionospheric dynamo region, *J. Geophys. Res.*, *113*, A02310, doi:10.1029/2007JA012737.

Fuller-Rowell, T. J., et al. (2008), Impact of terrestrial weather on the upper atmosphere, *Geophys. Res. Lett.*, *35*, L09808, doi:10.1029/2007GL032911.

Goncharenko, L., and S.-R. Zhang (2008), Ionospheric signatures of sudden stratospheric warming: Ion temperature at middle latitude, *Geophys. Res. Lett.*, *35*, L21103, doi:10.1029/2008GL035684.

Goncharenko, L., J. Chau, H.-L. Liu, and A. J. Coster (2010), Unexpected connections between the stratosphere and ionosphere, *Geophys. Res. Lett.*, *37*, L10101, doi:10.1029/2010GL043125.

Hagan, M. E., and R. G. Roble (2001), Modeling diurnal tidal variability with the National Center for Atmospheric Research thermosphere-ionosphere-mesosphere-electrodynamics general circulation model, *J. Geophys. Res.*, *106*, 24,869–24,882.

Hagan, M. E., M. D. Burrage, J. M. Forbes, J. Hackney, W. J. Randel, and X. Zhang (1999), GSWM-98: Results for migrating solar tides, *J. Geophys. Res.*, *104*, 6813–6828.

Hagan, M. E., A. Maute, and R. G. Roble (2009), Tropospheric tidal effects on the middle and upper atmosphere, *J. Geophys. Res.*, *114*, A01302, doi:10.1029/2008JA013637.

Holton, J. R., and H. Tan (1980), The influence of the equatorial quasi-biennial oscillation on the global circulation at 50 mb, *J. Atmos. Sci.*, *37*, 2200–2208.

Immel, T. J., E. Sagawa, S. L. England, S. B. Henderson, M. E. Hagan, S. B. Mende, H. U. Frey, C. M. Swenson, and L. J. Paxton (2006), Control of equatorial ionospheric morphology by atmospheric tides, *Geophys. Res. Lett.*, *33*, L15108, doi:10.1029/2006GL026161.

Laštovička, J., and D. Pancheva (1991), Changes in the characteristics of planetary waves at 80-100 km over central and southern Europe since 1980, *Adv. Space Res.*, *11*, 31–34.

Lei, J., J. P. Thayer, J. M. Forbes, E. K. Sutton, R. S. Nerem, M. Temmer, and A. M. Veronig (2008), Global thermospheric density variations caused by high-speed solar wind streams during the declining phase of solar cycle 23, *J. Geophys. Res.*, *113*, A11303, doi:10.1029/2008JA013433.

Lindzen, R. S. (1981), Turbulence and stress owing to gravity wave and tidal breakdown, *J. Geophys. Res.*, *86*, 9707–9714.

Liu, H.-L., E. R. Talaat, R. G. Roble, R. S. Lieberman, D. M. Riggin, and J.-H. Yee (2004), The 6.5 day wave and its seasonal variability in the middle and upper atmosphere, *J. Geophys. Res.*, *109*, D21112, doi:10.1029/2004JD004795.

Liu, H. L., et al. (2007), Comparative study of short term tidal variability, *J. Geophys. Res.*, *112*, D18108, doi:10.1029/2007JD008542.

Matsuno, T. (1971), A dynamical model of the stratospheric sudden warming, *J. Atmos. Sci.*, *28*, 1479–1494.

Meyer, C. K., and J. M. Forbes (1997), A 6.5 day westward propagating planetary wave: Origin and characteristics, *J. Geophys. Res.*, *102*, 26,173–26,178.

Mikhailov, A. V., A. K. Depueva, and T. Y. Leschinskaya (2004), Morphology of quiet time F2-layer disturbances: High and lower latitudes, *Int. J. Geomag. Aeronom.*, *1–14*, GI1004, doi:10.1029/2003GI000058.

Mikhailov, A. V., V. H. Depuev, and A. H. Depueva (2007), Synchronous NmF2 and NmE daytime variations as a key to the mechanism of quiet-time F2-layer disturbances, *Ann. Geophys.*, *25*, 483–493.

Nayar, S. R. P., T. J. Mathew, C. V. Sreehari, S. G. Sumod, C. V. Devasia, S. Ravindran, V. Sreeja, T. K. Pant, and R. Sridharan (2009), Electrodynamics of the equatorial F region ionosphere during pre-sunrise period, *Ann. Geophys.*, *27*, 107–111.

Pancheva, D., N. Mitchell, R. R. Clark, J. Drobjeva, and J. Laštovička (2002), Variability in the maximum height of the ionospheric F2-layer

over Millstone Hill (September 1998 to March 2000); influence from below and above, *Ann. Geophys*, *20*, 1807–1819.

Plumb, R. A. (1983), Baroclinic instability of the summer mesosphere: A mechanism for the quasi two day wave?, *J. Atmos. Sci.*, *40*, 262–270.

Pogoreltsev, A. I., A. A. Vlasov, K. Fröhlich, and C. Jacobi (2007), Planetary waves in coupling the lower and upper atmosphere, *J. Atmos. Sol. Terr. Phys.*, *69*, 2083–2101.

Richmond, A. D. (1983), Thermospheric dynamics and electrodynamics, in *Solar-Terrestrial Physics*, *Astrophys. Space Sci. Libr.*, vol. 104, edited by R. L. Carovillano and J. M. Forbes, p. 859, D. Reidel, Boston, Mass.

Richmond, A. D., E. C. Ridley, and R. G. Roble (1992), A thermosphere/ionosphere general circulation model with coupled electrodynamics, *Geophys. Res. Lett.*, *19*, 601–604.

Rishbeth, H., and M. Mendillo (2001), Patterns of ionospheric variability, *J. Atmos. Sol. Terr. Phys.*, *63*, 1661–1680.

Roble, R. G. (2000), On the feasibility of developing a global atmospheric model extending from the ground to the exosphere, in *Atmospheric Science Across the Stratopause*, *Geophys. Monogr. Ser.*, vol. 123, edited by D. E. Siskind, S. D. Eckermann, and M. E. Summers, p. 342, AGU, Washington, D. C.

Roble, R. G., and E. C. Ridley (1994), A thermosphere-ionosphere-mesosphere-electrodynamics general circulation model (TIME-GCM): Equinox solar cycle minimum simulations (30–500 km), *Geophys. Res. Lett.*, *21*, 417–420.

Roble, R. G., E. C. Ridley, A. D. Richmond, and R. E. Dickinson (1988), A coupled thermosphere/ionosphere general circulation model, *Geophys. Res. Lett.*, *15*, 1325–1328.

Sassi, F., D. Kinnison, B. A. Boville, R. R. Garcia, and R. G. Roble (2004), Effect of El Niño-Southern Oscillation on the dynamical, thermal, and chemical structure of the middle atmosphere, *J. Geophys. Res.*, *109*, D17108, doi:10.1029/2003JD004434.

Smith, A. K. (1996), Longitudinal variations in mesospheric winds: Evidence for gravity wave filtering by planetary waves, *J. Atmos. Sci.*, *53*, 1156–1173.

Takahashi, H., et al. (2007), Signatures of ultra fast Kelvin waves in the equatorial middle atmosphere and ionosphere, *Geophys. Res. Lett.*, *34*, L11108, doi:10.1029/2007GL029612.

Takeda, M., and T. Araki (1985), Electric conductivity of the ionosphere and nocturnal currents, *J. Atmos. Terr. Phys.*, *47*, 601–609.

Xiong, J., W. Wan, B. Ning, L. Liu, and Y. Gao (2006), Planetary wave-type oscillations in the ionosphere and their relationship to mesospheric/lower thermospheric and geomagnetic disturbances at Wuhan (30.61°N, 114.51°E), *J. Atmos. Sol. Terr. Phys.*, *68*, 498–508.

H.-L. Liu, A. D. Richmond, R. G. Roble, and W. Wang, High Altitude Observatory, National Center for Atmospheric Research, PO Box 3000, Boulder, CO 80307-3000, USA. (liuh@ucar.edu)